2023-01-31

A pseudo-static model for dynamic analysis on frequency domain of distributed compliant mechanisms

Mingxiang Ling
Xi'an Jiaotong University, ling_mx@163.com

Larry L. Howell
Brigham Young University - Provo, lhowell@byu.edu

June Cao
Xi'an Jiaotong University, caojy@mail.xjtu.edu.cn

Zhou Jiang
Xi'an Jiaotong University, jiangzhou_xy@163.com

Original Publication Citation

"Ling, M., Howell, L.L., Cao, J., Jian, Z., "A Pseudo-Static Model for Dynamic Analysis on Frequency Domain of Distributed Compliant Mechanisms," Journal of Mechanisms and Robotics, Vol 10, 051011-1 to 051011-10, doi: 10.1115/1.4040700, 2018."

A pseudo-static model for dynamic analysis on frequency domain of distributed compliant mechanisms

Mingxiang Ling[a, b]
[a] State Key Laboratory for Manufacturing Systems Engineering, Xi'an Jiaotong University, Xi'an 710049, China
[b] Institute of Systems Engineering, China Academy of Engineering Physics, Mianyang 621999, China
No.28, Mianshan road, Mianyang, China
ling_mx@163.com

Larry L. Howell[1]
Department of Mechanical Engineering, Brigham Young University, Provo, Utah, 84602, USA
435S CTB, Brigham Young University, Provo, UT
lhowell@byu.edu
ASME Membership

Junyi Cao
State Key Laboratory for Manufacturing Systems Engineering, Xi'an Jiaotong University, Xi'an 710049, China
No.64, Xianning road, Xi'an, China
caojy@mail.xjtu.edu.cn

Zhou Jiang
State Key Laboratory for Manufacturing Systems Engineering, Xi'an Jiaotong University, Xi'an 710049, China
No.64, Xianning road, Xi'an, China
jiangzhou_xy@163.com

ABSTRACT

This paper presents a pseudo-static modeling methodology for dynamic analysis of distributed compliant mechanisms to provide accurate and efficient solutions. First, a dynamic stiffness matrix of the flexible beam is deduced, which has the same definition and a similar form as the traditional

[1] Corresponding author: lhowell@byu.edu.

static compliance/stiffness matrix but is frequency-dependent. Second, the pseudo-static modeling procedure for the dynamic analysis is implemented in a statics-similar way. Then, all the kinematic, static and dynamic performances of compliant mechanisms can be analyzed based on the pseudo-static model. The superiority of the proposed method is that when it is used for the dynamic modeling of compliant mechanisms, the traditional dynamic modeling procedures, such as the calculation of elastic and kinetic energies as well as using the Lagrange's equation, are avoided and the dynamic modeling is converted to a statics-similar problem. Comparison of the proposed method with an elastic-beam-based model in previous literature and finite element analysis for an exemplary XY precision positioning stage reveals its high accuracy and easy operation.

Keywords: *compliant mechanisms, flexure hinge, precision positioning stage, compliance matrix, flexible manipulator*

1. INTRODUCTION

Compliant mechanisms have attracted widespread attention in a variety of scientific and industrial applications owing to their high precision and compact size without wear, friction, backlash or need little assembly [1]. However, one limitation of compliant mechanisms in comparison to their rigid-body counterparts is that the design and analysis of compliant mechanisms require simultaneous consideration of kinematic and elasto-mechanical behaviors. Hence, a considerable number of publications have been focused on this issue over the past decades. For example, the pseudo-rigid-body model (PRBM) proposed by Howell et al. [1, 2] has been widely developed to obtain an approximate solution of large deformation and used for static and dynamic analyses of compliant mechanisms by simplifying a flexure hinge as the joint with springs [3-5]. Recent developments of the beam-constraint model by Awtar and Chen et al. [6, 7] as

well as the multiple segment method by Su et al. [8] are also aimed for large deflection analysis. Additionally, plenty of linear methods are now available for the kinetostatic modeling of compliant mechanisms with small deformation, such as the elastic beam theory [9, 10], Castigliano's second theorem [11, 12] and the compliance-matrix-based method [13, 14]. With these methods, kinematics and statics of compliant mechanisms with simple and complex configurations [15-17] can now be well resolved.

Compared to the massive solutions available for large deformation and linear kinetostatic analysis of compliant mechanisms, fewer efforts have focused on the dynamics of compliant mechanisms in the past decades. The existing dynamic modeling methods can be generalized into three categories.

When the flexure hinge is simulated as a joint with springs and the dynamic model is established by simplifying a compliant mechanism as the rigid-body system, the version is known as the PRBM-based method [18-23]. For example, a PRBM-based dynamic model for parallel-guided compliant mechanism was developed by Yu et al. [18] based on dynamic equivalence; the stiffness of the flexure hinge was calculated by using PRBM and the dynamic model of a 3-DOF precision positioner was established based on Lagrange's equation in [19].

In the second category, Li et al. [24] employed the compliance matrix method to calculate the input/output stiffness of a compliant mechanism and a lumped-parameter dynamic model was built by Lagrange's equation; the input stiffness of a bridge-type displacement amplifier was calculated by using the Castigliano's second theorem and then a lumped-parameter dynamic model was built in [25]. All these solutions can be

classified as a lumped-parameter dynamic model [24-28], in which the equivalent stiffness of a compliant mechanism is usually calculated first by the aforementioned static methods, then the lumped-parameter dynamic model can be further established by computing the kinetic and elastic energies with the motion degree of freedom (DOF) as the variable.

The third category is termed the distributed-parameter model with finite DOFs [29-36], in which a compliant mechanism is often discretized into several elements and the dynamic model is established by calculating the total elastic and kinetic energies based on the Lagrange's equation. For example, a modeling method similar to the rigid-multi-body dynamics proposed by Ryu et al. [29] is now improved and used for designing precision manipulators by many groups [30-33]; more recently, a semi-analytical finite element model was developed by Ling et al. [34].

A brief summary of the characteristics and limitations of the aforementioned dynamic modeling methods is as follows:

I) The previous dynamic modeling is usually based on the Lagrange's equation and by calculating the kinetic and elastic energies. The question is whether it is possible to implement a dynamic modeling similar to the static procedure without employing the Lagrange's equation or Hamilton's principle? This will simplify the modeling complexity for compliant mechanisms, particularly considering the difficulty that simultaneous kinematic and elasto-mechanical behaviors are required for analyzing compliant mechanisms.

II) Usually the fundamental frequency can be obtained but high-order frequencies are

non-available in a lumped-parameter dynamic model. Even by Ryu's method [29] or the semi-analytical FEM [34], the prediction accuracy for high-order frequencies is limited. Particularly, the prediction accuracy of dynamics is hard to be guaranteed for complex compliant mechanisms with distributed compliance. So the question is whether it is possible to obtain high-order frequencies with a satisfactory accuracy? It is helpful to calculate the dynamic stiffness and is useful for dynamic optimization as well as vibration control due to low damping of compliant mechanisms [37].

The contribution of the present paper is to provide a pseudo-static model to address these two problems. With this method, the kinetostatic and dynamic modeling of compliant mechanisms can be concurrently implemented in a statics-similar way. Additionally, high-order frequencies can be obtained with an acceptable accuracy so as to make the technique useful for high-dynamic applications.

The rest of this paper is organized as follows. In Section 2, special consideration is given to the comparison of three kinds of compliance/stiffness matrices, two of which are commonly seen in the previous literature of compliant mechanisms; then, a dynamic stiffness matrix for the flexible beam is derived. In Section 3, the pseudo-static modeling procedure is introduced with an example. A verification arrangement by comparing the proposed method with an elastic-beam-based model in previous literature and FEM is presented in Section 4. Concluding remarks are provided at the end.

2. DYNAMIC STIFFNESS MATRIX OF THE FLEXIBLE BEAM

As the basic elements in compliant mechanisms, the compliance/stiffness matrix of the flexure hinge or the flexible beam has been extensively investigated [38-41]. These

matrices can be obtained by a variety of methods, such as the aforementioned elastic beam theory or Castigliano's theorem [11, 12]. Based on the compliance/stiffness matrix of the flexure hinge/flexible beam, kinetostatics of the whole compliant mechanism can be further modeled by employing different methods, such as the compliance-matrix-based method [13, 14] and the transfer matrix method according to the characteristics of different configurations.

Fig. 1 shows the differences and relations of three kinds of compliance/stiffness matrices. The compliance matrix of all kinds of flexure hinges featuring elliptical, corner-filleted, circular, and so on, have been intensively studied [38, 39]. The compliance matrix can be further transformed into a 'super' elemental stiffness matrix in the frame of FEM, which is much beneficial for the kinetostatic modeling of complex flexure-hinge-based compliant mechanisms, where only one element is needed to model the flexure hinge as a variable cross-section beam with enough accuracy [34, 40, 41].

The previous compliance matrix and the 'super' element stiffness matrix are accurate enough for the kinetostatic modeling of compliant mechanisms. When using these compliance/stiffness matrices for the dynamic modeling of compliant mechanisms, cumbersome calculations of the kinetic/elastic energies as well as using Lagrange's equation/Hamilton's principle are often required. The dynamic modeling accuracy is also limited by the simplification of mass distribution, especially for complex compliant mechanisms with distributed compliance. Given that concern, if the dynamic frequency is included into the compliance/stiffness matrices of the flexure hinge and the flexible beam, the dynamic modeling of the whole compliant mechanism would be simplified.

Such a frequency-dependent matrix is called 'dynamic stiffness matrix'. As illustrated in Fig. 1, it can be expected that the first term in the dynamic stiffness matrix will be equal to the static elemental stiffness matrix. Meanwhile, a dynamic compliance matrix that is frequency-dependent can also be obtained by taking the last three rows and last three columns in the dynamic stiffness matrix.

Distributed compliant mechanisms are the focus of this paper, thus the dynamic stiffness matrix of a flexible beam with uniform cross-section is deduced by solving the governing differential equations of vibration. As shown in Fig. 2, the flexible beam has two nodes j and k with three degrees of freedom per node, these being axial displacements u_j and u_k; transverse deflections w_j and w_k; rotations φ_j and φ_k. Then, the frequency-dependent relationship between the nodal force and nodal displacement of a flexible beam can be connected by the dynamic stiffness matrix $\boldsymbol{D}^e(\omega)$

$$\boldsymbol{F}^e(\omega)=\boldsymbol{D}^e(\omega)\cdot\boldsymbol{x}^e(\omega)=\begin{bmatrix} d_1 & 0 & 0 & d_5 & 0 & 0 \\ 0 & d_2 & -d_3 & 0 & d_6 & d_7 \\ & & d_4 & 0 & -d_7 & d_8 \\ & & & d_1 & 0 & 0 \\ & Sym & & & d_2 & d_3 \\ & & & & & d_4 \end{bmatrix}\cdot\boldsymbol{x}^e(\omega) \tag{1}$$

where nodal force $\boldsymbol{F}^e(\omega)=[F_{jx}, F_{jy}, M_j, F_{kx}, F_{ky}, M_k]^{\mathrm{T}}$, nodal displacement $\boldsymbol{x}^e(\omega)=[u_j, w_j, \varphi_j, u_k, w_k, \varphi_k]^{\mathrm{T}}$, ω is the dynamic frequency. By setting ω=0, $\boldsymbol{F}^e(\omega)$ and $\boldsymbol{x}^e(\omega)$ are actually the usual nodal force and nodal displacement.

Defining the physical parameters as follows: A and I are the area and moment of inertia about the neutral axis of the cross-section, E is the Young's modulus, ρ is the mass per unit length, $\alpha^2=\omega^2 l^2\rho/E$ and $\beta^4=\omega^2 l^4\rho A/EI$. The expression of $\boldsymbol{D}^e(\omega)$ in the

form of exact solutions and power series can be expressed as Eq. (2a) to Eq. (2h). The detailed derivation procedure is listed in the Appendix.

$$d_1 = \frac{EA\alpha\cot\alpha}{l} \approx \frac{EA}{l}\left(1-\sum_{n=1}^{\infty}\frac{2^{2n}}{(2n)!(2n+1)!}(\alpha l)^{2n}\right) \approx \frac{EA}{l}\left(1-\frac{1}{3}(\alpha)^2-\frac{1}{45}(\alpha)^4-\frac{2}{945}(\alpha)^6-\ldots\right) \tag{2a}$$

$$d_2 = \frac{EI\beta^3(\cos\beta\sinh\beta+\sin\beta\cosh\beta)}{l^3(1-\cos\beta\cosh\beta)} \approx \frac{EI}{l^3}\left(12-\frac{13}{35}(\beta)^4-\frac{59}{161700}(\beta)^8-\frac{551}{794593800}(\beta)^{12}-\ldots\right) \tag{2b}$$

$$d_3 = -\frac{EI\beta^2(\sin\beta\sinh\beta)}{l^2(1-\cos\beta\cosh\beta)} \approx -\frac{EI}{l^2}\left(6-\frac{11}{210}(\beta)^4-\frac{223}{2910600}(\beta)^8-\frac{3547}{23837814000}(\beta)^{12}-\ldots\right) \tag{2c}$$

$$d_4 = \frac{EI\beta(\sin\beta\cosh\beta-\cos\beta\sinh\beta)}{l(1-\cos\beta\cosh\beta)} \approx \frac{EI}{l}\left(4-\frac{1}{105}(\beta)^4-\frac{71}{4365900}(\beta)^8-\frac{127}{3972969000}(\beta)^{12}-\ldots\right) \tag{2d}$$

$$d_5 = -\frac{EA\alpha\csc\alpha}{l} \approx -\frac{EA}{l}\left(1+\sum_{n=1}^{\infty}\frac{(2^{2n}-1)}{(2n)!(2n+1)!}(\alpha l)^{2n}\right) \approx -\frac{EA}{l}\left(1+\frac{1}{6}(\alpha)^2+\frac{7}{360}(\alpha)^4+\frac{31}{15120}(\alpha)^6+\ldots\right) \tag{2e}$$

$$d_6 = -\frac{EI\beta^3(\sin\beta+\sinh\beta)}{l^3(1-\cos\beta\cosh\beta)} \approx -\frac{EI}{l^3}\left(12+\frac{9}{70}(\beta)^4+\frac{1279}{3880800}(\beta)^8+\frac{5801}{8475667200}(\beta)^{12}+\ldots\right) \tag{2f}$$

$$d_7 = \frac{EI\beta^2(\cosh\beta-\cos\beta)}{l^2(1-\cos\beta\cosh\beta)} \approx \frac{EI}{l^2}\left(6+\frac{13}{420}(\beta)^4+\frac{1681}{23284800}(\beta)^8+\frac{112631}{76810048000}(\beta)^{12}+\ldots\right) \tag{2g}$$

$$d_8 = \frac{EI\beta(\sinh\beta-\sin\beta)}{l(1-\cos\beta\cosh\beta)} \approx \frac{EI}{l}\left(2+\frac{1}{140}(\beta)^4+\frac{1097}{69854400}(\beta)^8+\frac{899}{28252224000}(\beta)^{12}+\ldots\right) \tag{2h}$$

By substituting the power series in Eq. (2a) ~ Eq. (2h) into $\boldsymbol{D}^e(\omega)$ in Eq. (1), the dynamic stiffness matrix of a flexible beam can be restructured in the form of series expansion

$$\boldsymbol{D}^e(\omega) = \boldsymbol{K}_0 - \omega^2\boldsymbol{M}_1 - \omega^4\boldsymbol{M}_2 - \omega^6\boldsymbol{M}_3 - \ldots \tag{3}$$

in which, $\boldsymbol{K}_0$ is the first term that is equal to the static elemental stiffness matrix in Fig. 1. $\boldsymbol{M}_1$, $\boldsymbol{M}_2$, $\boldsymbol{M}_3$, …, are the constant coefficient matrices that can be directly obtained from the series expansion in Eq. (2a) to Eq. (2h). $\boldsymbol{K}_0$ and $\boldsymbol{M}_1$ are respectively listed in Eq. (4) and Eq. (5) to illustrate their equalities to the traditional static elemental stiffness matrix

and the consistent mass matrix in FEM. If high-order terms in Eq. (3) are omitted, the dynamic stiffness matrix is degenerated into the traditional dynamic model, i.e. $\boldsymbol{D}^e(\omega)=\boldsymbol{K}_0-\omega^2\boldsymbol{M}_1$. This means solving a dynamic problem using the static stiffness matrix and the consistent mass matrix is equivalent to considering only the first two terms in Eq. (3) and all the high-order terms are ignored. Since the coefficients in $\boldsymbol{M}_2$, $\boldsymbol{M}_3$, …, are small, this approximation is reasonable as long as the frequency is low and the length of the flexible beam is small. This explains why some traditional dynamic models always lead to unrealistic prediction for high-order frequencies.

$$\boldsymbol{K}_0=\frac{E}{l^3}\begin{bmatrix} Al^2 & 0 & 0 & -Al^2 & 0 & 0 \\ & 12I & 6Il & 0 & -12I & 6Il \\ & & 4Il^2 & 0 & -6Il & 2Il^2 \\ & & & Al^2 & 0 & 0 \\ & Sym & & & 12I & -6Il \\ & & & & & 4Il^2 \end{bmatrix} \tag{4}$$

$$\boldsymbol{M}_1=\frac{\rho Al}{420}\begin{bmatrix} 140 & 0 & 0 & 70 & 0 & 0 \\ & 156 & 22l & 0 & 54 & -13l \\ & & 4l^2 & 0 & 13l & -3l^2 \\ & & & 140 & 0 & 0 \\ & Sym & & & 156 & -22l \\ & & & & & 4l^2 \end{bmatrix} \tag{5}$$

It is of significance that the dynamic stiffness matrix of a flexible beam accounts for an infinite number of natural frequencies with desired accuracy. This is, of course, not the case in traditional dynamic modeling methods. On the other hand, with the dynamic stiffness matrix, the dynamic modeling of a compliant mechanism can be performed without calculating the kinetic and elastic energies. The so-called pseudo-static modeling method is introduced next.

3. THE PSEUDO-STATIC MODELING METHOD

3.1 Modeling Procedure

Fig. 3 provides the general procedure of the pseudo-static model for concurrently kinetostatic and dynamic analyses of compliant mechanisms. In the first step, a compliant mechanism is discretized into the flexure hinge, the flexible beam and the lumped mass according to its configuration. The lumped mass is the part bearing little deformation compared to the other two parts. The flexure hinge is not discussed in this paper for distributed compliant mechanisms; the dynamic stiffness matrix of the flexible beam is shown in Eq. (1) and Eq. (2) and that of the lumped mass is

$$\boldsymbol{m}(\omega)=\begin{bmatrix} -m\omega^2 & 0 & 0 \\ 0 & -m\omega^2 & 0 \\ 0 & 0 & -J\omega^2 \end{bmatrix} \tag{6}$$

where *m* and *J* are, respectively, the mass and the mass moment of inertia.

In the second step, since the dynamic stiffness matrix has the same definition and a similar form as the static elemental stiffness matrix, the pseudo-static model of the whole compliant mechanism can be built by using previous static modeling methods. If necessary, a frequency-dependent compliance matrix can be established by taking the last three rows and three columns in the dynamic stiffness matrix, so the compliance-matrix-based static methods, such as that in [13, 14], can be easily implemented for the dynamic modeling without adopting Lagrange's method. The ultimate pseudo-static model of the whole compliant mechanism will have the form of

$$\left[\boldsymbol{D}(\omega)\right]\cdot\left\{\boldsymbol{X}(\omega)\right\}=\left\{\boldsymbol{F}(\omega)\right\} \tag{7}$$

where $\boldsymbol{D}(\omega)$ is the dynamic stiffness matrix of the whole compliant mechanism, $\boldsymbol{X}(\omega)$ and

$\boldsymbol{F}(\omega)$ are the selected displacement vector and the actuating force in the frequency domain. By letting ω=0, $\boldsymbol{X}(\omega)$ and $\boldsymbol{F}(\omega)$ are the usual variables in the static model.

Lastly, kinematic, static and dynamic performances can be analyzed based on Eq. (7) after considering boundary conditions, details are illustrated in Fig. 3. Of which, a transcendental or polynomial eigenproblem is required to solve the natural frequencies. Plenty of algorithms are available for eigenvalue solutions and the most simple may be the existing zero-root seeking functions in MATLAB. Wittrick-Williams algorithm [42] is also recommended because no natural frequencies are missed with this algorithm.

3.2 Pseudo-Static Model for an XY Precision Positioning Stage

In this subsection, a distributed compliant mechanism is employed to illustrate the detailed pseudo-static modeling procedure. The device schematic is shown in Fig. 4 (a). The motions in the two DOFs are kinematically decoupled by the flexible beams (marked as blue in Fig. 4 (a)) and it has the same static and dynamic performances in the *x*- and *y*-directions.

As shown in Fig. 4 (b), the stage is discretized into the flexible beam and lumped mass. They are denoted serially from (1) to (34) and are connected with nodes from 1 to 19; all the clamped nodes are numbered as 0. The pseudo-static model of the stage is established by using the matrix displacement method here but other static modeling methods are feasible. To this end, the nodal force and nodal displacement of the *i*th flexible beam in the reference system are first expressed based on Eq. (1) as

$$\begin{Bmatrix} \boldsymbol{F}_{i,j}(\omega) \\ \boldsymbol{F}_{i,k}(\omega) \end{Bmatrix} = \left(\boldsymbol{R}_i^{\mathrm{T}} \cdot \boldsymbol{D}_i^e(\omega) \cdot \boldsymbol{R}_i \right) \cdot \begin{Bmatrix} \boldsymbol{x}_j(\omega) \\ \boldsymbol{x}_k(\omega) \end{Bmatrix} = \left(\boldsymbol{R}_i^{\mathrm{T}} \cdot \begin{bmatrix} \boldsymbol{k}_{i,1} & \boldsymbol{k}_{i,2} \\ \boldsymbol{k}_{i,3} & \boldsymbol{k}_{i,4} \end{bmatrix} \cdot \boldsymbol{R}_i \right) \cdot \begin{Bmatrix} \boldsymbol{x}_j(\omega) \\ \boldsymbol{x}_k(\omega) \end{Bmatrix} \tag{8}$$

where $\boldsymbol{F}_{i,j}(\omega)=[F_{jx}, F_{jy}, M_j]^{\mathrm{T}}$ and $\boldsymbol{F}_{i,k}(\omega)=[F_{kx}, F_{ky}, M_k]^{\mathrm{T}}$ are the two nodal forces of the ith flexible beam in the reference system. $\boldsymbol{x}_j=[u_j, w_j, \varphi_j]^{\mathrm{T}}$ and $\boldsymbol{x}_k=[u_k, w_k, \varphi_k]^{\mathrm{T}}$ are the two nodal displacements in the reference system. $\boldsymbol{k}_{i,1}$, $\boldsymbol{k}_{i,2}$, $\boldsymbol{k}_{i,3}$ and $\boldsymbol{k}_{i,4}$ are the block sub-matrices of the dynamic stiffness matrix, $\boldsymbol{D}_i^e(\omega)$, of the flexible beam and can be expressed as

$$\boldsymbol{k}_{i,1}=\begin{bmatrix} d_1 & 0 & 0 \\ 0 & d_2 & -d_3 \\ 0 & -d_3 & d_4 \end{bmatrix}, \boldsymbol{k}_{i,2}=\boldsymbol{k}_{i,3}^{\mathrm{T}}=\begin{bmatrix} d_5 & 0 & 0 \\ 0 & d_6 & d_7 \\ 0 & -d_7 & d_8 \end{bmatrix} \boldsymbol{k}_{i,4}=\begin{bmatrix} d_1 & 0 & 0 \\ 0 & d_2 & d_3 \\ 0 & d_3 & d_4 \end{bmatrix} \tag{9}$$

where the values of d_i (i=1,2,…,8) are assigned in Eq. (2a) to Eq. (2h).

In Eq. (8), transformation matrix $\boldsymbol{R}_i$ is determined by the orientation of the ith flexible beam with respect to the reference system (denoted as θ_i) and can be written as

$$\boldsymbol{R}_i=\begin{bmatrix} \cos\theta_i & \sin\theta_i & 0 & 0 & 0 & 0 \\ -\sin\theta_i & \cos\theta_i & 0 & 0 & 0 & 0 \\ 0 & 0 & 1 & 0 & 0 & 0 \\ 0 & 0 & 0 & \cos\theta_i & \sin\theta_i & 0 \\ 0 & 0 & 0 & -\sin\theta_i & \cos\theta_i & 0 \\ 0 & 0 & 0 & 0 & 0 & 1 \end{bmatrix} \tag{10}$$

Taking each node (from 1 to 19) as the study object, the force exerted on the node by its connected flexible beams is the sum of the inverse nodal force of those flexible beams. Thus, the following force balance equation can be obtained for the nth node

$$\sum\nolimits_N\left[\left(\boldsymbol{F}_{i,j}(\omega) \text{ or } \boldsymbol{F}_{i,k}(\omega)\right)\right]+\boldsymbol{m}_n\boldsymbol{x}_n=\boldsymbol{P}_n \tag{11}$$

where N is the number of flexible beams connected to the nth node. Since the nth node may be connected to the j-end or the k-end of the ith flexible beam as shown in Fig. 4 (b), so $\boldsymbol{F}_{i,j}(\omega)$ is selected if the nth node is connected to the j-end; otherwise $\boldsymbol{F}_{i,k}(\omega)$ is valid. $\boldsymbol{m}_n$ is the dynamic stiffness matrix of the lumped mass shown in Eq. (6), this term is

included only when the *n*th node is assumed as a lumped mass. $\boldsymbol{P}_n$ is the sum of external forces directly exerted on the *n*th node and the equivalent force from intra-force in the reference system. For the mechanism in Fig. 4, the piezo-actuated force F_p is assumed to directly exert on nodes 2, 6, 15 and 18.

By substituting the nodal force in Eq. (11) with the dynamic stiffness matrix and the nodal displacement in Eq. (8), the following equilibrium equation can be obtained for the *n*th node

$$\sum\nolimits_N \left[\left((\boldsymbol{k}_{i,1}\boldsymbol{x}_j + \boldsymbol{k}_{i,2}\boldsymbol{x}_k) \text{ or } (\boldsymbol{k}_{i,3}\boldsymbol{x}_j + \boldsymbol{k}_{i,4}\boldsymbol{x}_k) \right) \right] + \boldsymbol{m}_n \boldsymbol{x}_n = \boldsymbol{P}_n \tag{12}$$

where the former is selected if the *n*th node is connected to the *j*-end of the *i*th flexible beam; the latter is valid when the force exerted on the node is from the *k*-end.

Eq. (12) is the force equilibrium equation of the *n*th node. Representative node 2 and node 4 in Fig. 4 (b) are selected to illustrate the detailed equilibrium equation

$$\begin{cases} \text{node 2:} \quad \boldsymbol{k}_{2,3}\boldsymbol{x}_1 + (\boldsymbol{k}_{2,4} + \boldsymbol{k}_{3,1})\boldsymbol{x}_2 + \boldsymbol{k}_{3,2}\boldsymbol{x}_3 = \left[0, F_p, 0\right]^{\mathrm{T}} \\ \text{node 4:} \quad \boldsymbol{k}_{4,3}\boldsymbol{x}_3 + (\boldsymbol{k}_{4,4} + \boldsymbol{k}_{5,1} + \boldsymbol{k}_{9,4} + \boldsymbol{k}_{10,4} + \boldsymbol{k}_{11,1} + \boldsymbol{k}_{12,1} + \boldsymbol{m}_4)\boldsymbol{x}_4 + \boldsymbol{k}_{5,2}\boldsymbol{x}_5 + (\boldsymbol{k}_{11,2} + \boldsymbol{k}_{12,2})\boldsymbol{x}_8 = \boldsymbol{0} \end{cases} \tag{13}$$

In Eq. (13), $\boldsymbol{m}_4$ is included because node 4 is a lumped mass. The balance equation for other nodes can be similarly obtained based on Eq. (12) but are omitted here. Considering the force balance of all nodes in sequence similar to Eq. (13), the pseudo-static model of the whole compliant mechanism by taking the nodal displacements as the variable can be established as

$$\boldsymbol{D}(\omega)\cdot\boldsymbol{X}(\omega) = \boldsymbol{F}(\omega) \text{ i.e. } \begin{bmatrix} \boldsymbol{k}_{1,4} + \boldsymbol{k}_{2,1} & \boldsymbol{k}_{2,2} & \boldsymbol{0} & \cdots & \boldsymbol{0} \\ \boldsymbol{k}_{2,3} & \boldsymbol{k}_{2,4} + \boldsymbol{k}_{3,1} & \boldsymbol{k}_{3,2} & \cdots & \boldsymbol{0} \\ \vdots & \vdots & \vdots & \vdots & \vdots \\ \boldsymbol{0} & \boldsymbol{0} & \boldsymbol{0} & \cdots & \boldsymbol{k}_{33,4} + \boldsymbol{k}_{34,4} \end{bmatrix} \cdot \begin{Bmatrix} \boldsymbol{x}_1 \\ \boldsymbol{x}_2 \\ \vdots \\ \boldsymbol{x}_{19} \end{Bmatrix} = \begin{Bmatrix} \boldsymbol{P}_1 \\ \boldsymbol{P}_2 \\ \vdots \\ \boldsymbol{P}_{19} \end{Bmatrix} \tag{14}$$

where $\boldsymbol{X}(\omega)=[\boldsymbol{x}_1, \boldsymbol{x}_2, \cdots, \boldsymbol{x}_{19}]^{\mathrm{T}}$, $\boldsymbol{F}(\omega)=[\boldsymbol{P}_1, \boldsymbol{P}_2, \cdots, \boldsymbol{P}_{19}]^{\mathrm{T}}$, $\boldsymbol{D}(\omega)$ is the dynamic stiffness matrix of the whole precision positioning stage.

Eq. (14) describes the pseudo-static model of the exemplary precision positioning stage by taking the nineteen nodal displacement vectors as the variable. By letting dynamic frequency, ω, to be zero, the kinematic and static performances, such as the displacement amplification ratio, R, and the input stiffness, K_{in}, in the x-direction can be calculated as

$$R=\frac{\boldsymbol{x}_{8(x)}}{(\boldsymbol{x}_{2(y)}-\boldsymbol{x}_{6(y)})},\ K_{in}=\frac{F_p}{-\boldsymbol{x}_{6(y)}}=\frac{F_p}{\boldsymbol{x}_{2(y)}} \tag{15}$$

where $\boldsymbol{x}_{8(x)}$ and $\boldsymbol{x}_{n(y)}$ (n=2, 6) are the nodal displacements in the x- and y-directions.

As to the natural frequencies of the XY precision positioning stage, it is the roots of the determinant of the total dynamic stiffness matrix, $\boldsymbol{D}(\omega)$, in Eq. (14), i.e.

$$\det\left(\boldsymbol{D}(\omega)\right)=0 \tag{16}$$

Moreover, the forced frequency response and time response of the XY precision positioning stage can be calculated based on the following inverse matrix operation and inverse Fourier transform

$$\begin{cases}\boldsymbol{X}(\omega)=\boldsymbol{D}^{-1}(\omega)\cdot\boldsymbol{F}(\omega)\\ \boldsymbol{X}(t)=IFFT\left(\boldsymbol{D}^{-1}(\omega)\cdot\boldsymbol{F}(\omega)\right)\end{cases} \tag{17}$$

It should also be noted that the displacement frequency response, $\boldsymbol{H}_d(\omega)$, which describes the dynamic displacement characteristics of the compliant mechanism can be expressed as

$$\boldsymbol{H}_d(\omega)=\frac{\boldsymbol{X}(\omega)}{\boldsymbol{F}(\omega)}=\boldsymbol{D}^{-1}(\omega) \tag{18}$$

In this paper, linear and un-damped vibration of the compliant mechanism is considered, so the dynamic responses of velocity and acceleration in the frequency domain, $\boldsymbol{H}_v(\omega)$ and $\boldsymbol{H}_a(\omega)$, can be directly obtained as

$$\begin{cases} \boldsymbol{H}_v(\omega) = \dfrac{\boldsymbol{V}(\omega)}{\boldsymbol{F}(\omega)} = \dfrac{\omega \cdot \boldsymbol{X}(\omega)}{\boldsymbol{F}(\omega)} = \omega \cdot \boldsymbol{D}^{-1}(\omega) \\ \boldsymbol{H}_a(\omega) = \dfrac{\boldsymbol{A}(\omega)}{\boldsymbol{F}(\omega)} = \dfrac{\omega^2 \cdot \boldsymbol{X}(\omega)}{\boldsymbol{F}(\omega)} = \omega^2 \cdot \boldsymbol{D}^{-1}(\omega) \end{cases} \tag{19}$$

where $\boldsymbol{V}(\omega)$ and $\boldsymbol{A}(\omega)$ are respectively the output velocity and output acceleration of the compliant mechanism in the frequency domain.

From the preceding modeling procedure for the illustrative compliant mechanism, it can be seen that only a few steps and concise equations are needed to perform the kinematic, static and dynamic analyses of a compliant mechanism based on the pseudo-static model. All these analyses can be implemented together with easy operation but not the traditional way where static and dynamic modeling are usually separate. Besides, the traditional dynamic modeling procedures, such as calculating the kinetic and elastic energies as well as using the Lagrange's equation, are avoided.

4. NUMERICAL VERIFICATION AND DISCUSSION

The static performance, the first six natural frequencies and the forced dynamic response of the XY precision positioning stage in Fig. 4 were calculated with (i) the proposed pseudo-static model, (ii) the elastic-beam-based model in [43] and (iii) the finite element method (FEM) to verify the proposed method. For finite element analysis, the precision positioning stage was geometrically modeled using Pro/E software, then static analysis, modal analysis and harmonic response were carried out with the

commercial software package ANSYS. The Solid185 element was chosen to build the model and the local mesh was refined. The element size was set as 1 mm and the results were proven to be convergent and accurate enough. Aluminum was selected as the material and the physical parameters are listed in Table 1. For static calculation in ANSYS, a concentrated actuation force of 100 N was exerted on the interface of the input ports of the stage. The *x*-component of the displacements of node 2 and node 6 were used as the input displacement in the proposed method, accordingly the central displacement of the input ports was read in the finite elemental analysis. For forced dynamic response calculation by the proposed method and FEM, an impulse response with the magnitude of 100 N was carried out.

4.1 Static Performance

Fig. 5 provides the theoretical results of the displacement amplification ratio with the proposed method and the elastic model in [43] as well as four sets of numerical results from ANSYS. The theoretical results of the input stiffness with the proposed method and four sets of numerical results from ANSYS are shown in Fig. 6. Quantitative results are listed in Table 2 with a comparison between the proposed method and FEM. One can see that the pseudo-static model matches well with the results of FEM in the whole range of changes of the geometric parameter. The maximum deviation is less than 6.4% for eight sets of data. The high accuracy is due to the fact that there is little approximation during the derivation of the pseudo-static model.

On the other hand, the elastic model in [43] doesn't match well with the results of the proposed pseudo-static model and those from FEM, as shown in Fig. 5. The main

reason for the large error of the elastic model in [43] is that input ports of the compliant mechanism are assumed to be rigid during modeling, while the input ports are modeled as to be flexible both in the pseudo-static model and FEM. To illustrate this difference, the displacement amplification ratio was calculated again by the pseudo-static model under different thickness of the input ports (h_2=4 mm, 8 mm and 12 mm) and the results are shown in Fig. 7. It can be seen that with the increasing of the thickness, which means the input ports become more and more rigid, the results of the pseudo-static model gradually approach to the results of the elastic model in [43]. The results also indicate the significant influence of the compliance of input ports on the static performance of compliant mechanisms and the compliance of input ports should be seriously considered in device design.

4.2 Natural Frequencies

The first six natural frequencies were calculated for a comparison between the pseudo-static model and the finite element method. The first six vibration modes are shown in Fig. 8 and the natural frequencies are comparatively listed in Table 3. One can see that the fundamental frequencies in the *x*- and *y*-directions are the same and can be accurately predicted by the pseudo-static model with the deviations of only 0.9%; the prediction errors are less than 5% for the high-order natural frequencies except for the fourth vibration mode, the deviation for this mode reaches up to 12.2%. The large error may be that the Bernoulli-Euler theory used in the dynamic stiffness matrix can not exactly describe the local stiffening effect in the fourth vibration mode. It should also be noted that the prediction accuracy for high-order vibration modes would be further

enhanced if the shear effects, the rotational moment or other significant factors are considered. On the other hand, the computing time for the first six natural frequencies with the example is less than 0.15 s (the code was not optimized and the calculation was implemented with an ordinary laptop of 2 GB memory). This aspect can represent a great advantage in time-critical scenarios, such as the dynamic optimization or real-time feedback controller design.

4.3 Forced dynamic response

To demonstrate the forced dynamic response of the pseudo-static model, dynamic response analysis was carried out by using the pseudo-static model and the harmonic response in ANSYS. Actuating impulse force with the magnitude of 100 N and frequency range from 1 Hz to 4000 Hz was exerted on the interface of the input ports of the precision positioning stage in the *x*-direction. Displacement, velocity and acceleration of the central platform in this direction were selected as the output responses and were calculated by Eq. (18) and Eq. (19). The actuating frequency range fully covers the first six-order natural frequencies of the XY precision positioning stage. Fig. 9 comparatively provides the dynamic response by the two methods, and four conclusions can be obtained:

- In the low frequency domain, which represents the static performance of the XY precision positioning stage, the output responses from the two methods match well. This has already been verified in the preceding static analysis.
- The two main resonance frequencies actuated by the input impulse are actually the first-order and fifth-order natural frequencies of the positioning stage. This

can be easily understood from the vibration modes in Fig. 8 that both of those two modes are in the x-direction. The pseudo-static model matches well with FEM for the dynamic response with the maximum error of 3.5%.

- From the enlarged view, one can see that the third and fourth vibration modes are slightly activated and their influence on the forced dynamic response is small. This can be easily understood from the vibration modes in Fig. 8 that both of those two modes are not in the target motion direction. Although the deviation for the fourth vibration mode between the two methods is 12.2% as shown in Table 3, this mode just slightly contributes to the forced dynamic response, so prediction accuracy of the forced dynamic response by the pseudo-static model is not largely affected.
- The resonance frequencies of displacement, velocity and acceleration in the forced dynamic response are identical and also equal to the calculated natural frequencies in subsection 4.2 (listed in Table 3). The results are consistent with the theory of vibration. It should be noted that the resonance frequencies of displacement, velocity and acceleration will be unequal for damped dynamics and large deformation.

4.4 Comments on the Advantages and Limitations of the Pseudo-Static Model

As is well known, only the fundamental frequency of compliant mechanisms can be calculated with the previous lumped-parameter models; the prediction accuracy is also hard to ensure for complex configurations with distributed compliance since too much simplification of mass will lead to uncontrollable error. Although high-order frequencies

can be obtained by the multi-rigid-body or finite-element-based methods, such as the Ryu's method [29] or the semi-analytical FEM [34], their accuracy for high-order frequencies is also unsatisfactory, in which the displacement is approximated by static shape function. Actually, the displacement shape function not only relates to the spatial coordinate but also to the frequency in harmonic vibration. Moreover, calculating the kinetic and elastic energies of a compliant mechanism along with using the Lagrange's equation are often required in the previous dynamic modeling methods; those routines, however, are all avoided when the pseudo-static model is utilized for the dynamic modeling of compliant mechanisms.

The core of the proposed pseudo-static model is to establish a suitable frequency-dependent dynamic stiffness matrix for the flexure hinge/flexible beam. The governing equation of vibration based on the Bernoulli-Euler beam was adopted in this paper, but some other factors, such as the shear deflection, rigid rotation, axial force and large deformation, could also be further considered and included into the dynamic stiffness matrix for specific compliant mechanisms. On the other hand, a transcendental or polynomial eigenproblem for solving natural frequencies is required in the pseudo-static model. Possible modal truncation techniques to simplify this analysis could be further investigated and an explicit fundamental frequency formula for some simple compliant mechanisms would be convenient for fast evaluation of dynamic performance during the initial stage of design.

5. CONCLUSIONS

This paper presents a new approach aimed at efficiently solving the dynamic modeling problem of distributed compliant mechanisms. This method is based on the dynamic stiffness matrix of flexible beams, which has the same definition and a similar form as the traditional static compliance/stiffness matrices but is frequency-dependent. Different from the previous dynamic modeling methods for compliant mechanisms in which calculation of the kinetic and elastic energies as well as using the Lagrange's equation are needed, the kinetostatic and dynamic modeling of compliant mechanisms can be concurrently implemented in a concise statics-similar way based on the proposed method. Comparative calculations of the static performance, the first six-order natural frequencies and the forced dynamic response for an XY precision positioning stage with the proposed method, the elastic model in previous literature and FEM demonstrate the accuracy and efficiency of the pseudo-static model.

FUNDING

This work was supported by the National Natural Science Foundation of China (grant numbers 51705487, 51575426), China; and the State Key Laboratory Program of Xi'an Jiaotong University (grant number SV2016-KF-19), China.

NOMENCLATURE

$\boldsymbol{C}$	Compliance matrix of the flexure hinge/flexible beam
$\boldsymbol{K}$	Stiffness matrix of the flexure hinge/flexible beam
l	Length of the flexure hinge/flexible beam
$\boldsymbol{K}_0$	Elemental stiffness matrix of the flexure hinge/flexible beam in the frame of FEM
$\boldsymbol{D}^e(\omega)$	Dynamic stiffness matrix of the flexure hinge/flexible beam
$\boldsymbol{F}^e(\omega, t)$	Nodal force of the flexible beam
$\boldsymbol{x}^e(t)$	Nodal displacement of the flexible beam
ω	Dynamic frequency
t	Time
A	Area of the cross-section of the flexure hinge/flexible beam
I	Moment of inertia about the neutral axis of the cross-section
E	Young's modulus
ρ	Mass per unit length
$\boldsymbol{D}(\omega)$	Dynamic stiffness matrix of the whole compliant mechanism
$\boldsymbol{X}(\omega)$	Selected displacement vector of the whole compliant mechanism
$\boldsymbol{F}(\omega)$	Actuating force of the whole compliant mechanism
$\boldsymbol{R}_i$	Coordinate transformation matrix

$\boldsymbol{P}_n$	The sum of forces directly exerted on the nth node
F_p	Piezoelectric actuating force
R	Displacement amplification ratio of the whole compliant mechanism
K_{in}	Input stiffness of the whole compliant mechanism

REFERENCES

[1] Howell, L. L., 2001, *Compliant Mechanisms*, John Wiley & Sons.

[2] Howell, L. L., and Midha, A, 1994, "A Method for the Design of Compliant Mechanisms with Small-Length Flexural Pivots," ASME Journal of Mechanical Design, **116**(1), pp. 280-290.

[3] Su, H. J., 2009, "A Pseudo-Rigid-Body 3R Model for Determining Large Deflection of Cantilever Beams Subject to Tip Loads," ASME Journal of Mechanisms and Robotics, **1**(2), DOI: 021008.

[4] Midha, A., Bapat, S. G., Mavanthoor, A., and Chinta, V., 2015, "Analysis of a Fixed-Guided Compliant Beam with an Inflection Point Using the Pseudo-Rigid-Body Model Concept," ASME Journal of Mechanisms and Robotics, **7**(3), DOI: 031007.

[5] Calogero, J., Frecker, M., Hasnain, Z., and Hubbard, J. E., 2018, "Tuning of a Rigid-Body Dynamics Model of a Flapping Wing Structure with Compliant Joints," ASME Journal of Mechanisms and Robotics, **10**(1), DOI: 011007.

[6] Awtar, S., and Sen, S., 2010, "A Generalized Constraint Model for Two-Dimensional Beam Flexures: Nonlinear Load-Displacement Formulation," ASME Journal of Mechanical Design, **132**(8), DOI: 081008.

[7] Chen, G., and Bai, R., 2016, "Modeling Large Spatial Deflections of Slender Bisymmetric Beams in Compliant Mechanisms Using Chained Spatial-Beam Constraint Model," ASME Journal of Mechanisms and Robotics, **8**(4), DOI: 041011.

[8] Turkkan, O. A., and Su, H. J., 2017, "A General and Efficient Multiple Segment Method for Kinetostatic Analysis of Planar Compliant Mechanisms," Mechanism and Machine Theory, **112**, pp. 205-217.

[9] Kurita, Y., Sugihara, F., Ueda, J., and Ogasawara, T., 2012, "Piezoelectric Tweezer-Type End Effector with Force-and Displacement-Sensing Capability," IEEE/ASME Transactions on Mechatronics, **17**(6), pp. 1039-1048.

[10] Ling, M., Cao, J., Zeng, M., Lin, J., and Inman, D. J., 2016, "Enhanced Mathematical Modeling of the Displacement Amplification Ratio for Piezoelectric Compliant Mechanisms," Smart Materials and Structures, **25**(7), pp. 75022-75032.

[11] Lobontiu, N., and Garcia, E., 2003, "Analytical Model of Displacement Amplification and Stiffness Optimization for a Class of Flexure-Based Compliant Mechanisms," Computers & structures, **81**(32), pp. 2797-2810.

[12] Yong, Y. K., and Leang, K. K., 2016, *Mechanical Design of High-Speed Nanopositioning Systems*, Springer International Publishing, In Nanopositioning Technologies, pp. 61-121.

[13] Li, Y., and Xu, Q., 2010, "Development and Assessment of a Novel Decoupled XY Parallel Micropositioning Platform," IEEE/ASME Transactions on Mechatronics, **15**(1), PP. 125-135.

[14] Koseki, Y., Tanikawa, T., Koyachi, N., and Arai, T., 2002, "Kinematic Analysis of a Translational 3-DOF Micro-Parallel Mechanism Using the Matrix Method," Advanced Robotics, **16**(3), pp. 251-264.

[15] Choi, K. B., Lee, J. J., Kim, G. H., Lim, H. J., and Kwon, S. G., 2018, "Amplification Ratio Analysis of a Bridge-Type Mechanical Amplification Mechanism Based on a Fully Compliant Model," Mechanism and Machine Theory, **121**, pp. 355-372.

[16] Lobontiu, N., 2014, "Compliance-Based Matrix Method for Modeling the Quasi-Static Response of Planar Serial Flexure-Hinge Mechanisms," Precision Engineering, **38**(3), pp. 639-650.

[17] Jiang, Y., Li, T. M., and Wang, L. P., 2015, "Stiffness Modeling of Compliant Parallel Mechanisms and Applications in the Performance Analysis of a Decoupled Parallel Compliant Stage," Review of Scientific Instruments, **86**(9), DOI: 095109.

[18] Yu, Y. Q., Howell, L. L., Lusk, C., Yue, Y., and He, M. G., 2005, "Dynamic Modeling of Compliant Mechanisms Based on the Pseudo-Rigid-Body Model," ASME Journal of Mechanical Design, **127**(4), pp. 760-765.

[19] Guo, Z., Tian, Y., Liu, C., Wang, F., Liu, X., Shirinzadeh, B., and Zhang, D., 2015, "Design and Control Methodology of a 3-DOF Flexure-Based Mechanism for Micro/Nano-Positioning," Robotics and Computer-Integrated Manufacturing, **32**, PP. 93-105.

[20] Chen, W., Qu, J., Chen, W., and Zhang, J., 2017, "A Compliant Dual-Axis Gripper with Integrated Position and Force Sensing," Mechatronics, **47**, pp. 105-115.

[21] Xu, Q., 2013, "Design, Testing and Precision Control of a Novel Long-Stroke Flexure Micropositioning System," Mechanism and Machine Theory, **70**, pp. 209-224.

[22] Wang, F., Liang, C., Tian, Y., Zhao, X., and Zhang, D., 2015, "Design of a Piezoelectric-Actuated Microgripper with a Three-Stage Flexure-Based Amplification," IEEE/ASME Transactions on Mechatronics, **20**(5), pp. 2205-2213.

[23] Li, Y., and Wu, Z., 2016, "Design, Analysis and Simulation of a Novel 3-DOF Translational Micromanipulator Based on the PRB Model," Mechanism and Machine Theory, **100**, pp. 235-258.

[24] Tang, H., and Li, Y., 2014, "Development and Active Disturbance Rejection Control of a Compliant Micro-/Nanopositioning Piezostage with Dual Mode," IEEE Transactions on Industrial Electronics, **61**(3), pp. 1475-1492.

[25] Zhu, X., Xu, X., Wen, Z., Ren, J., and Liu, P., 2015, "A Novel Flexure-Based Vertical Nanopositioning Stage with Large Travel Range," Review of Scientific Instruments, **86**(10), DOI: 105112.

[26] Zhu, W. L., Zhu, Z., Guo, P., and Ju, B. F., 2018, "A Novel Hybrid Actuation Mechanism Based XY Nanopositioning Stage with Totally Decoupled Kinematics," Mechanical Systems and Signal Processing, **99**, pp. 747-759.

[27] Polit, S., and Dong, J., 2011, "Development of a High-Bandwidth XY Nanopositioning Stage for High-Rate Micro-/Nanomanufacturing," IEEE/ASME Transactions on Mechatronics, **16**(4), pp. 724-733.

[28] Liu, P., Yan, P., and Zhang, Z., 2015, "Design and Analysis of an X–Y Parallel Nanopositioner Supporting Large-Stroke Servomechanism," Proceedings of the Institution of Mechanical Engineers, Part C: Journal of Mechanical Engineering Science, **229**(2), pp. 364-376.

[29] Ryu, J. W., Lee, S. Q., Gweon, D. G., and Moon, K. S., 1999, "Inverse Kinematic Modeling of a Coupled Flexure Hinge Mechanism," Mechatronics, **9**(6), pp. 657-674.

[30] Choi, S. B., Han, S. S., Han, Y. M., and Thompson, B. S., 2007, "A Magnification Device for Precision Mechanisms Featuring Piezoactuators and Flexure Hinges: Design and Experimental Validation," Mechanism and Machine Theory, **42**(9), pp. 1184-1198.

[31] Kim, H., and Gweon, D. G., 2012, "Development of a Compact and Long Range XYθz Nano-Positioning Stage," Review of Scientific Instruments, **83**(8), pp. 085102.

[32] Lai, L. J., and Zhu, Z. N., 2017, "Design, Modeling and Testing of a Novel Flexure-Based Displacement Amplification Mechanism," Sensors and Actuators A: Physical, **266**, pp. 122-129.

[33] Lee, H. J., Kim, H. C., Kim, H. Y., and Gweon, D. G., 2013, "Optimal Design and Experiment of a Three-Axis Out-of-Plane Nano Positioning Stage Using a New Compact Bridge-Type Displacement Amplifier," Review of Scientific Instruments, **84**(11), DOI: 115103.

[34] Ling, M., Cao, J., Jiang, Z., and Lin, J., 2017, "A Semi-Analytical Modeling Method for the Static and Dynamic Analysis of Complex Compliant Mechanism," Precision Engineering.

[35] Rösner, M., Lammering, R., and Friedrich, R., 2015, "Dynamic Modeling and Model Order Reduction of Compliant Mechanisms," Precision Engineering, **42**, pp. 85-92.

[36] Shen, Y., Chen, X., Jiang, W., and Luo, X., 2014, "Spatial Force-Based Non-Prismatic Beam Element for Static and Dynamic Analyses of Circular Flexure Hinges in Compliant Mechanisms," Precision Engineering, **38**(2), pp. 311-320.

[37] Pereira, E., Aphale, S. S., Feliu, V., and Moheimani, S. R., 2011, "Integral Resonant Control for Vibration Damping and Precise Tip-Positioning of a Single-Link Flexible Manipulator," IEEE/ASME Transactions on Mechatronics, **16**(2), pp. 232-240.

[38] Lobontiu, N., Paine, J. S., Garcia, E., and Goldfarb, M., 2001, "Corner-Filleted Flexure Finges," ASME Journal of Mechanical Design, **123**(3), pp. 346-352.

[39] Yong, Y. K., Lu, T. F., and Handley, D. C., 2008, "Review of Circular Flexure Hinge Design Equations and Derivation of Empirical Formulations," Precision Engineering, **32**(2), pp. 63-70.

[40] Wang, H., and Zhang, X., 2008, "Input Coupling Analysis and Optimal Design of a 3-DOF Compliant Micro-Positioning Stage," Mechanism and Machine Theory, **43**(4), pp. 400-410.

[41] Cao, L., Dolovich, A. T., and Zhang, W. C., 2015, "Hybrid Compliant Mechanism Design Using a Mixed Mesh of Flexure Hinge Elements and Beam Elements Through Topology Optimization," ASME Journal of Mechanical Design, **137**(9), DOI: 092303.

[42] Banerjee, J. R., and Williams, F. W., 1985, "Exact Bernoulli–Euler Dynamic Stiffness Matrix for a Range of Tapered Beams," International Journal for Numerical Methods in Engineering, **21**(12), pp. 2289-2302.

[43] Ling, M., Cao, J., Jiang, Z., and Lin, J., 2017, "Modular Kinematics and Statics Modeling for Precision Positioning Stage," Mechanism and Machine Theory, 107, pp. 274-282.

APPENDIX

The governing differential equation of the longitudinal free vibration of a flexible beam can be expressed as

$$EAu'' - \rho A\ddot{u} = 0 \tag{A.1}$$

where $u(x, t)$ is the longitudinal displacement. The prime denotes the derivative with respect to spatial coordinate x and the superimposed dot indicates differentiation with respect to time t.

The eigenvalue equation in the spectral domain for Eq. (A.1) is

$$U'' + \lambda^2 U = 0 \tag{A.2}$$

where $\lambda^2 = \omega^2 \rho / E$, U is the shape function of the flexible beam and its solution can be expressed as

$$U = C_1 \cos \lambda x + C_2 \sin \lambda x \tag{A.3}$$

As shown in Fig. 2, by substituting the displacement boundary conditions, i.e. $U\big|_{x=0} = u_j$, $U\big|_{x=l} = u_k$ into Eq. (A.3), then the shape function can be solved as the expression of the nodal displacement

$$U = \left(\cos \lambda x - \cot \lambda l \cdot \sin \lambda x\right) \cdot u_j + \left(\csc \lambda l \cdot \sin \lambda x\right) \cdot u_k \tag{A.4}$$

The axial nodal force of the flexible beam is $F_{u,j} = -EAU'\big|_{x=0}$, $F_{u,k} = EAU'\big|_{x=l}$, so the following Eq. (A.5) can be deduced based on Eq. (A.4) and $\alpha = \lambda l$, which represents the relationship between the nodal force and nodal displacement in the form of dynamic stiffness matrix

$$\begin{Bmatrix} F_{u,j} \\ F_{u,k} \end{Bmatrix} = \frac{EA}{l} \alpha \begin{bmatrix} \cot \alpha & -\csc \alpha \\ -\csc \alpha & \cot \alpha \end{bmatrix} \cdot \begin{Bmatrix} u_j \\ u_k \end{Bmatrix} \tag{A.5}$$

The governing differential equation of free bending vibration of a Bernoulli-Euler beam can be expressed as

$$EIw'''' + \rho A\ddot{w} = 0 \tag{A.6}$$

where $w(x, t)$ is the bending displacement.

With a similar derivation procedure as the longitudinal vibration, the dynamic stiffness matrix of the bending vibration of a flexible beam can be deduced as

$$\begin{Bmatrix} F_{w,j} \\ M_j \\ F_{w,k} \\ M_k \end{Bmatrix} = \frac{EI}{l^3} \begin{bmatrix} B_1 & B_2 l & -B_3 & B_4 l \\ & B_5 l^2 & -B_4 l & B_6 l^2 \\ & & B_1 & -B_2 l \\ sym & & & B_5 l^2 \end{bmatrix} \cdot \begin{Bmatrix} w_j \\ \varphi_j \\ w_k \\ \varphi_k \end{Bmatrix} \tag{A.7}$$

where $\begin{cases} B_1 = \beta^3(\sin\beta\cosh\beta + \cos\beta\sinh\beta)/\phi \\ B_2 = \beta^2(\sinh\beta\sin\beta)/\phi \\ B_3 = \beta^3(\sinh\beta + \sin\beta)/\phi \\ B_4 = \beta^2(\cosh\beta - \cos\beta)/\phi \\ B_5 = \beta(\sin\beta\cosh\beta - \cos\beta\sinh\beta)/\phi \\ B_6 = \beta(\sinh\beta - \sin\beta)/\phi \\ \phi = 1 - \cosh\beta\cos\beta \end{cases}$.

By combining the longitudinal and the bending dynamic stiffness matrices, i.e. Eq. (A.5) and Eq. (A.7) into a uniform matrix, then Eq. (1) and Eq. (2) in Section 2 can be obtained.

Figure Captions List

Table Caption List

Figure List

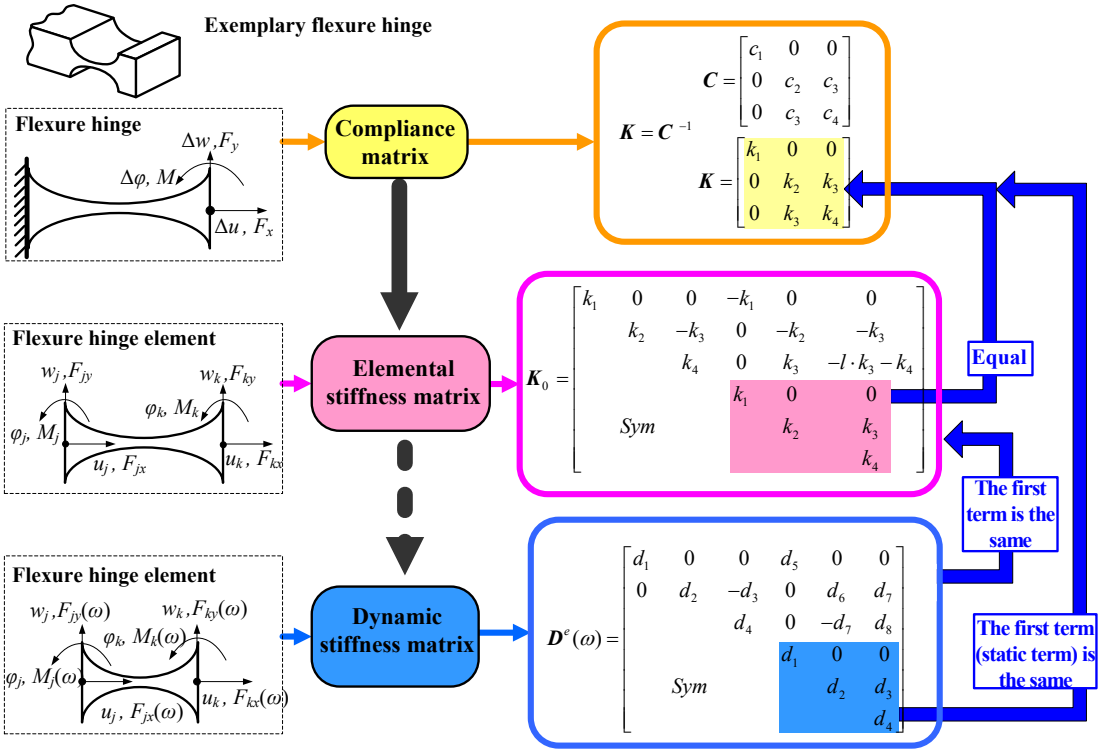

Fig. 1 Comparison of three kinds of compliance/stiffness matrices of the flexure hinge or the flexible beam.

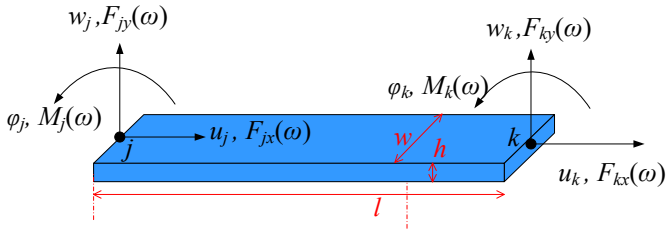

Fig. 2 Nodal displacement and nodal force of the flexible beam.

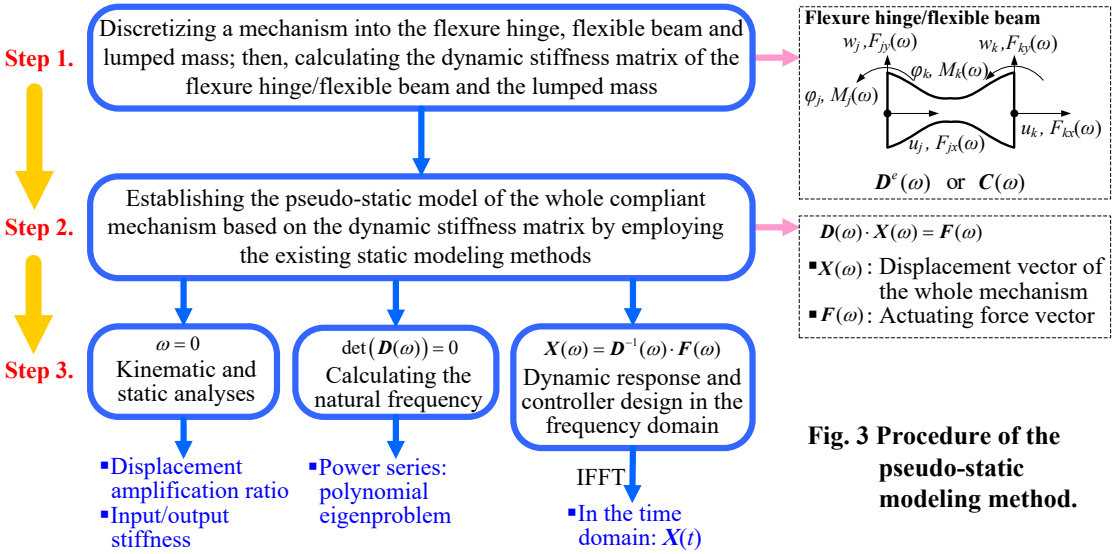

Fig. 3 Procedure of the pseudo-static modeling method.

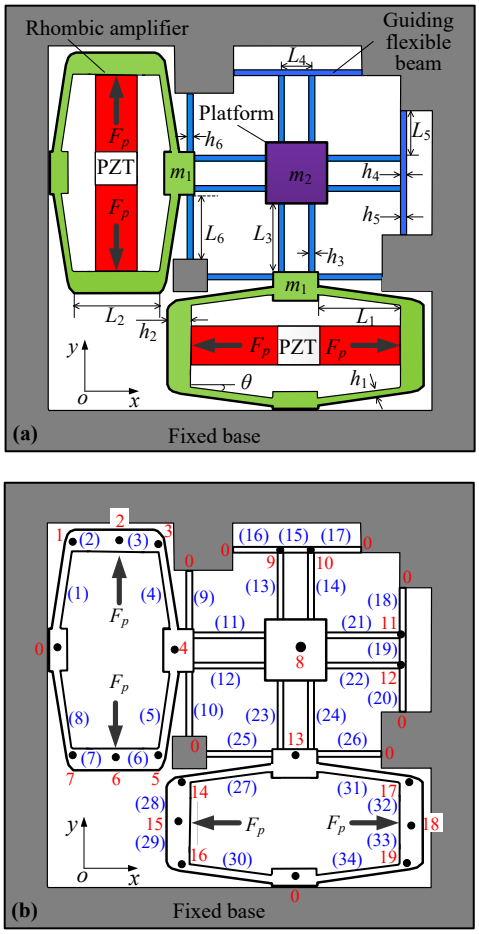

Fig. 4 Pseudo-static modeling of an XY monolithic precision positioning stage. (a) Schematic of the example. (b) Numbering of sub-elements.

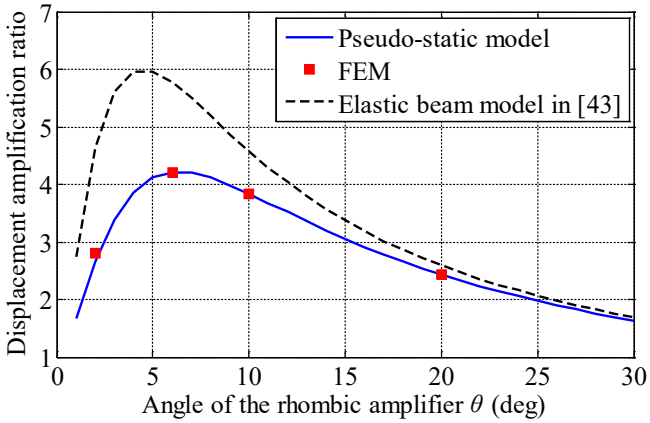

Fig. 5 Results of the displacement amplification ratio with different methods.

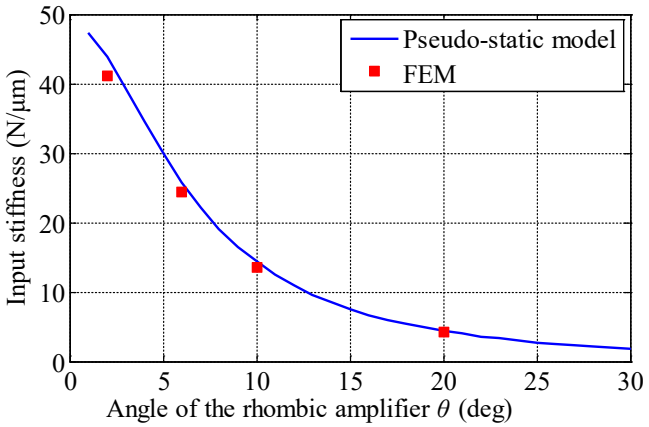

Fig. 6 Results of the input stiffness with different methods.

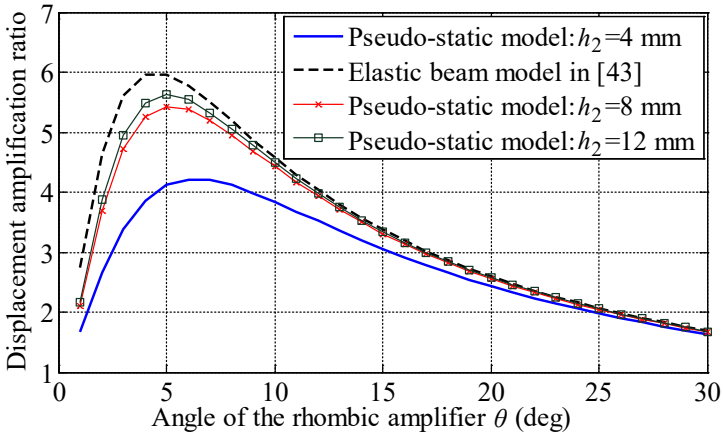

Fig. 7 Influence of the thickness of the input ports on the static performance.

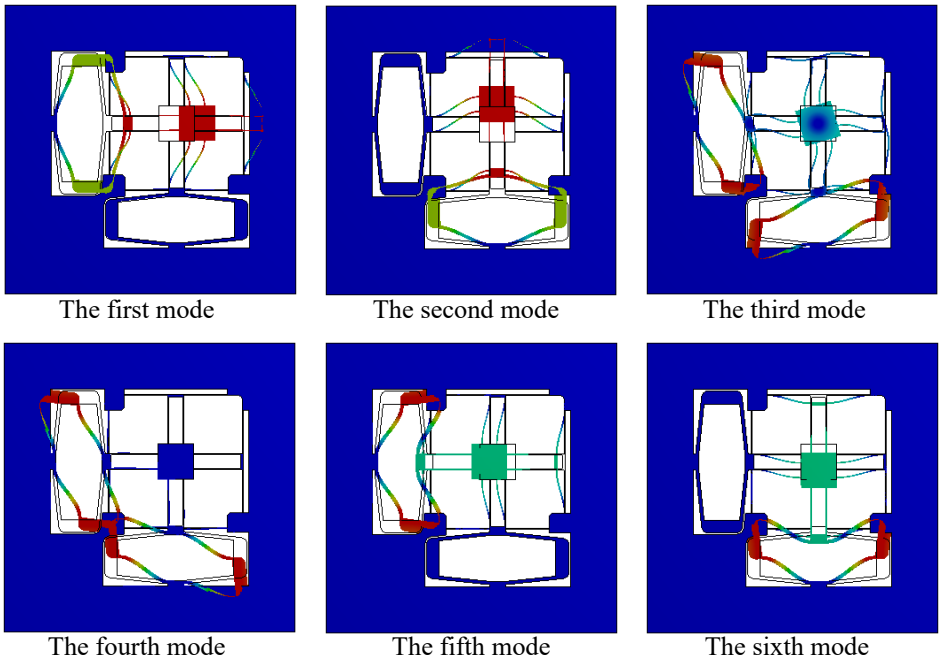

Fig. 8 The first six vibration modes calculated by FEM.

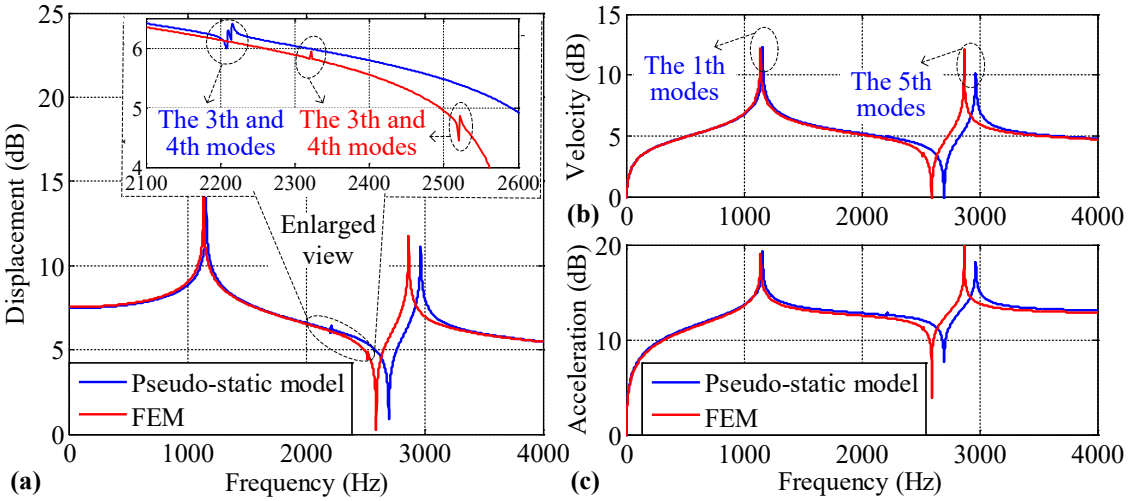

Fig. 9 Comparison of the forced dynamic response. (a) Output displacement. (b) Output velocity. (c) Output acceleration.

Table List

Table 1 Key geometric and material parameters

Parameters	Values	Parameters	Values
h_1 (mm)	1	L_5 (mm)	13.5
L_1 (mm)	15.5	h_6 (mm)	0.4
h_2 (mm)	4	L_6 (mm)	14.5
L_2 (mm)	12	d (mm)	10
h_3 (mm)	0.4	θ (deg)	6
L_3 (mm)	14.5	m_1 (g)	0.41
h_4 (mm)	1	m_2 (g)	3.35
L_4 (mm)	4.6	E (GPa)	71
h_5 (mm)	0.5	ρ (kg/m^3)	2770

Table 2 Results of the displacement amplification ratio with different methods

Angle θ (deg)	Displacement amplification ratio: R			Input stiffness: K_{in} (N/μm)		
	The pseudo-static model	FEM	Error	The pseudo-static model	FEM	Error
2	2.66	2.80	5.0%	43.83	41.18	6.4%
6	4.21	4.22	0.2%	25.84	24.42	5.8%
10	3.84	3.83	0.3%	14.31	13.60	5.2%
20	2.43	2.43	0.0%	4.38	4.22	3.8%

Table 3 Results of the natural frequencies with different methods

Natural frequencies	The pseudo-static model	FEM	Error
Mode 1	1149 Hz	1139 Hz	0.9%
Mode 2	1149 Hz	1142 Hz	0.6%
Mode 3	2206 Hz	2322 Hz	4.9%
Mode 4	2212 Hz	2520 Hz	12.2%
Mode 5	2965 Hz	2867 Hz	3.5%
Mode 6	2965 Hz	2869 Hz	3.3%